SciDAC ISEP simulations of energetic particle confinement in ITER

1st quarter report for FES Theory Performance Target (TPT), FY2022
December 31, 2021

Z. Lin for ISEP team and ITP B.11.12 team

Project summary

"Energetic particle confinement properties of ITER operation scenarios will be comprehensively assessed using global gyrokinetic codes, hybrid MHD codes, and reduced EP transport models"

1st quarter (10/21-12/21) milestones

"Evaluate linear instabilities of AEs, microinstabilities, and MHD modes in DIII-D and ITER"

During the first quarter of this project, we have evaluated linear instabilities in two ITER scenarios of broad interest and two matching DIII-D experiments. These four cases have been simulated by 9 first-principles codes (3 gyrokinetic, 3 kinetic-MHD, and 3 eigenvalue) for linear instabilities of MHD modes, Alfven eigenmodes (AEs), and microinstabilities. Key simulation results (Table 1) are:

- The n=1 fishbones driven by energetic particles (EP) are unstable in ITER baseline (BL) scenario and associated DIII-D validation case, but stable in ITER steady state (SS) scenario and associated DIII-D validation case. The n=1 kink modes are stable in all four cases.
- Various AEs including BAE, RSAE, and TAE driven by EP are unstable in all four cases with a large range of $10<n<50$ in ITER and a smaller range of $n<10$ in DIII-D.
- The high-n electrostatic driftwaves driven by thermal plasmas are strongly unstable in all four cases. The dominant microinstability in the core is trapped electron modes (TEM) in all cases, except for the ITER SS scenario which is dominated by ion temperature gradient (ITG) modes.

Several observations can be made from these simulation results:

- Effects of fishbones on EP redistribution in ITER BL and AEs on EP transport in ITER BL and SS need to be further evaluated by nonlinear simulations and transport modeling. Nonlinear interactions between different modes could be important considering the presence of multiple modes with similar growth rates, especially for ITER cases. Effects of microturbulence on fishbones and AEs could be important.
- The two DIII-D validation cases match reasonably well with the two ITER scenarios regarding linear instabilities of MHD, AEs, and microinstabilities. Linear simulation results of DIII-D cases are consistent with experimental observations of unstable modes.

	Baseline (BL)		Steady state (SS)	
	ITER	DIII-D	ITER	DIII-D
n=1 MHD mode	Fishbone	Fishbone	No instability	No instability
Meso-scale AE	BAE, RSAE, TAE n=4-50	BAE, RSAE, TAE n=1-11	RSAE, TAE, EAE n=6,40	BAE, RSAE, TAE n=6-9
Microinstability	TEM n=100-250	TEM n=30-50	ITG n=75-150	TEM n=20-50

Table 1. *Summary of linear instability found by simulations of ITER BL/SS scenarios and associated DIII-D validation cases.*

1. Introduction

Energetic particle transport in burning plasmas can be induced by macroscopic MHD modes, meso-scale Alfven eigenmode/energetic particle modes, and microturbulence, which could interact nonlinearly and therefore require integrated simulations. In this TPT2022 project, energetic particle confinement properties of ITER operation scenarios will be comprehensively assessed using global gyrokinetic codes, hybrid MHD codes, and reduced EP transport models. These integrated simulations incorporating multiple physical processes will be first verified and validated for simulations of EP transport through all channels in DIII-D experiments designed to simulate the ITER scenarios. This project has also been selected as an ITPA energetic particle physics joint activity (B.11.12), which uses modelling and experiments in present tokamaks to determine if fast particle instabilities will occur and need be controlled in 7.5MA/2.65T ITER H-modes with NBI heating. This collaborative research is coordinated by the SciDAC ISEP Center.

The ITER scenarios are selected for this study based on the criteria that they are of broad interest to ITER and ITPA community and may be prone to large energetic particle (EP) transport. After extensive discussions by the EP community at two recent ITER-EP meetings, two ITER scenarios (baseline and steady state) have been selected and IMAS equilibrium data have been provided by researchers at the ITER headquarter (S. Pinches, S. Kim, A. Polevoi et al) have selected two ITER scenarios.

To provide a validation for the ITER simulations, two existing DIII-D shots with similar safety factor and EP instabilities in the two ITER scenarios have been selected by experimental collaborators (W. Heidbrink et al). New experiments for better profile matching and parameter scan have been requested for DIII-D runtime in 2022. The comparisons of simulation results between DIII-D experiments and ITER scenarios can further provide physics insights on the extrapolation from existing fusion experiments to the future burning plasma experiments.

2. Equilibria (drafted by N. Gorelenkov)

The two ITER equilibria (including magnetic geometry, plasma profiles, and EP distribution) have been retrieved from IMAS database by N. Gorelenkov and made available to all participating codes at the following Google drive:
https://drive.google.com/drive/folders/1ERTNpYTKkt6KEwnyG2wN0vAj48GGgDKl?usp=sharing

2.1. Baseline scenario

The baseline scenario is also the ITPA case ITER baseline shot #101006, which has the same hydrogen main plasma and beam ion species. It is a pre-fusion power operation or PFPO which seems to be the easiest case to simulate [*NF* **61**, 076008 (2021)]. For the comparison with the existing DIII-D experiments the baseline target case was also identified, which is the shot #178631. This DIII-D shot has weakly driven instabilities and matched the safety factor profile to ITER relevant scenario. In this discharge a similar value of density and its profile was measured. A variation of beam power and its direction was applied which made the modes unstable but not too strongly. The following spectrogram was measured in that shot which shows an AE activity from t=1200-1400msec, chirping frequency BAE activity from t=1200-1550msec, and the low frequency fishbones at the point of interest, t=1570msec when almost all the Alfvenic frequency activity is stabilized.

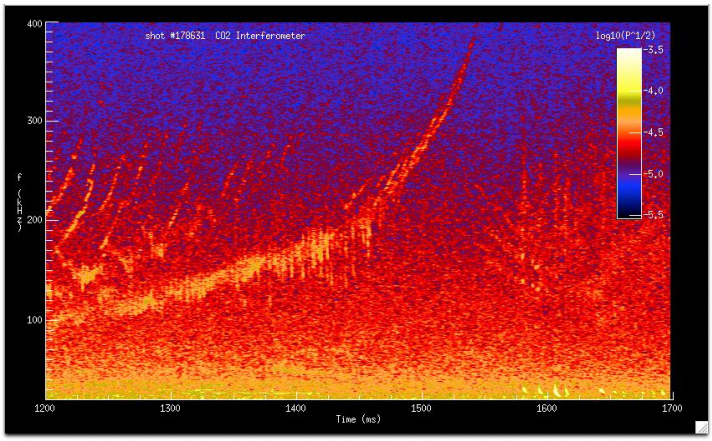

Fig.1 *CO2 interferometer spectrogram of DIII-D baseline scenario shot #178631. The time slice of interest is t=1570msec.*

For the comparison with ITER planned scenarios a safety factor profile seems to match ITER predicted profile quite nicely as it is shown in the following figure 2. The safety factor is close to 1 so that IMAS predicts that the plasma will be sawtoothing and some finite variations of the safety profile near unity is expected.

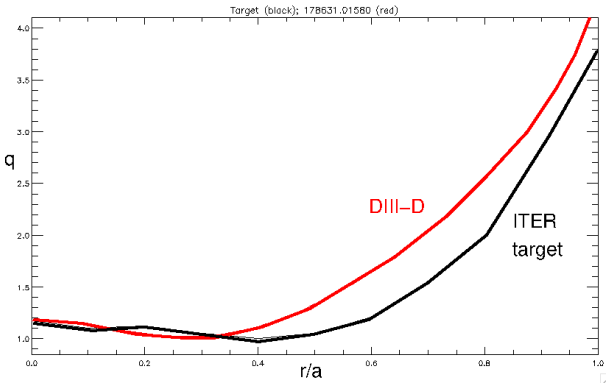

Fig.2 *The comparison of the safety factor profiles of DIII-D (#178631) and ITER (target, black) baseline scenarios (#101006).*

2.2. Steady state scenario

The ITER steady state scenario is shot # 131041 and the corresponding DIII-D experiment is shot # 132710, which has plenty of Alfvenic activities as shown in Fig.3.

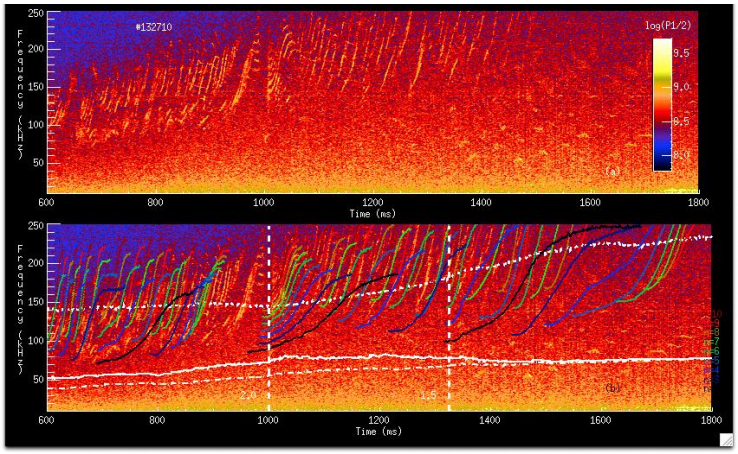

Fig.3. *CO2 interferometer spectrogram of a multitude of low frequency Alfvenic activity in DIII-D shot # 132710.*

In this DIII-D steady state shot safety profile is well fit to the expected ITER q-profile as shown in Fig. 4. The safety factor has a weakly reversed shear in the core of the DIII-D experiment, but a much stronger reversed shear in the ITER.

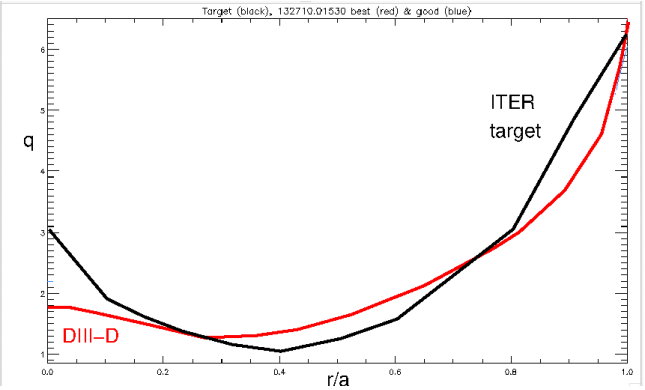

Fig.4 *The comparison of the safety factor profiles of DIII-D and ITER (target, black) steady state scenarios. The time slice to be used in simulations is the red curve corresponding to t=1530 msec of shot #132710.*

3. Macroscopic (n=1) MHD mode (drafted by G. Brochard)

The linear instability of the n=1 macroscopic MHD modes in the ITER baseline and steady state scenarios has been analyzed using the gyrokinetic code **GTC** (G. Brochard), kinetic-MHD code **M3D-C1** (C. Liu), and ideal MHD eigenvalue code **GAM-solver** (J. Bao). In the ideal MHD limit, the two configurations are found by all three codes to be stable for the kink modes, consistently with previous results obtained from the eigenvalue code KINX. The steady state scenario remains stable when thermal and fast ion kinetic effects are considered in the GTC and M3D-C1 simulations. On the other hand, a fishbone instability is found in the baseline case in the GTC simulation when including kinetic effects of thermal and beam ions, as shown in Fig. 5a-5b. We note that the mode only becomes unstable when a realistic anisotropic slowing-down distribution, as opposed to a local Maxwellian distribution, is considered for the NBI beam. The mode is driven mostly by energetic passing particles through a drift-transit resonance.

The two DIII-D experiments are also found to be stable by all three codes in the ideal MHD limit for the kink modes. The steady state case is stable as well with ion kinetic effects, while a fishbone mode is unstable for the baseline one (Fig. 5c-5d) when realistic NBI distributions are considered in both GTC and M3D-C1 simulations, similarly to the ITER plasma and consistent with the DIII-D experimental measurements. The mode structure in the DIII-D plasma is similar to the ITER one with both m=1 and 2 harmonics. The mode is found to be resonantly driven by both passing and trapped energetic particles. Results between GTC and M3D-C1 only agree qualitatively (Fig. 5d), as different NBI distributions have been considered between the codes. Further work with identical distributions will be performed.

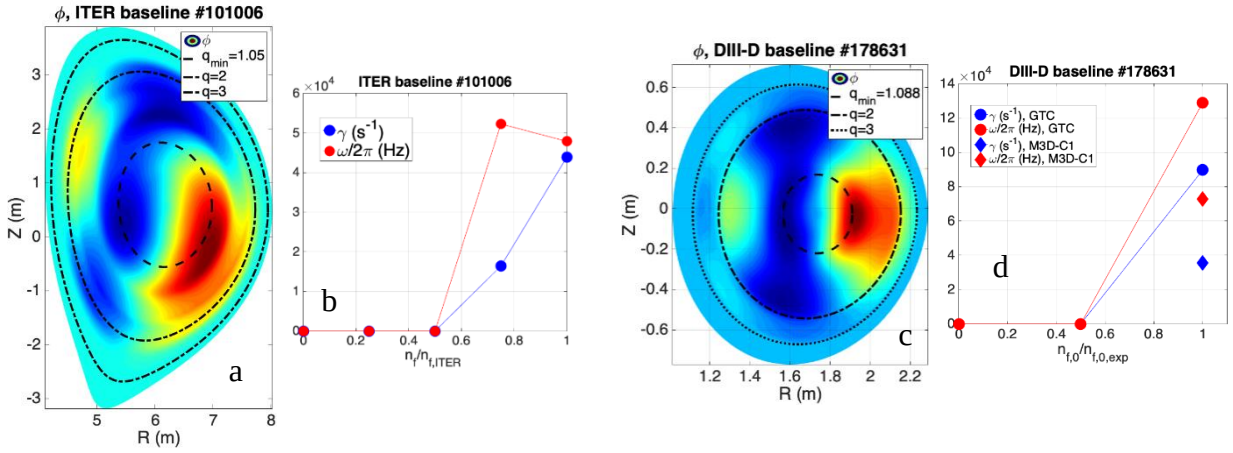

Fig. 5: (a,c) Electrostatic potential and (b,d) growth rates and mode frequencies for the fishbone instability in the ITER (a-b) and DIII-D (c-d) baseline scenarios.

4. Meso-scale Alfven eigenmode (drafted by E. Bass)

Alfvén eigenmode linear stability has been explored with seven codes: **GTC (P. Liu), GYRO (E. Bass), LIGKA** (T. Hayward-Schneider)**, NOVA-K** (N. Gorelenkov)**, M3D-C1** (C. Liu)**, FAR3D** (D. Spong), **MEGA** (Y. Todo), and **ORB5** (T. Hayward-Schneider). Each of the four cases (ITER baseline 101006 and steady-state 131041 and associated DIII-D discharges, 178631 for baseline and 132710 for steady-state) have so far been explored by some of the codes.

4.1. Baseline scenario

The ITER baseline case 101006 has been studied at by GTC, FAR3D, ORB5, and M3D-C1. The initial-value FAR3D simulations boosts the beam-ion drive strength to be able to easily see unstable AEs. Without FLR effects, robust AEs were seen up to n=50 (the highest tested). With finite-orbit effects, the growth rates go down dramatically, with the highest unstable mode seen at n=20. M3D-C1 finds highly unstable AEs ($\gamma/\omega \approx 0.1$) peaking at n=14, with n=18 the highest unstable n. The kinetic code ORB5 sees a tentatively-identified RSAE driven by thermal electrons without the beam. The DIII-D baseline shot was simulated by NOVA-K, GYRO, GTC, and M3D-C1. All codes find unstable AEs peaking around n=9,10. Some counter-propagating modes (electron diamagnetic direction) are observed in GYRO below n=5. Growth rates vary, with M3D-C1 predicting the highest growth rates due to absence of thermal kinetic damping mechanisms.

4.1.1. ITER

FAR3D was run in initial-value mode for this case. The EP drive was enhanced by a factor of 2.8 to more easily identify the unstable eigenmodes, although this enhancement is not expected to be necessary when using the eigenvalue solver. However, inclusion of finite-orbit physics is found to dramatically reduce AE growth rates, even below the nominal gyro-average turnover value of n=15. This implies the instability may be absent without the EP drive enhancement. See Fig. 6.

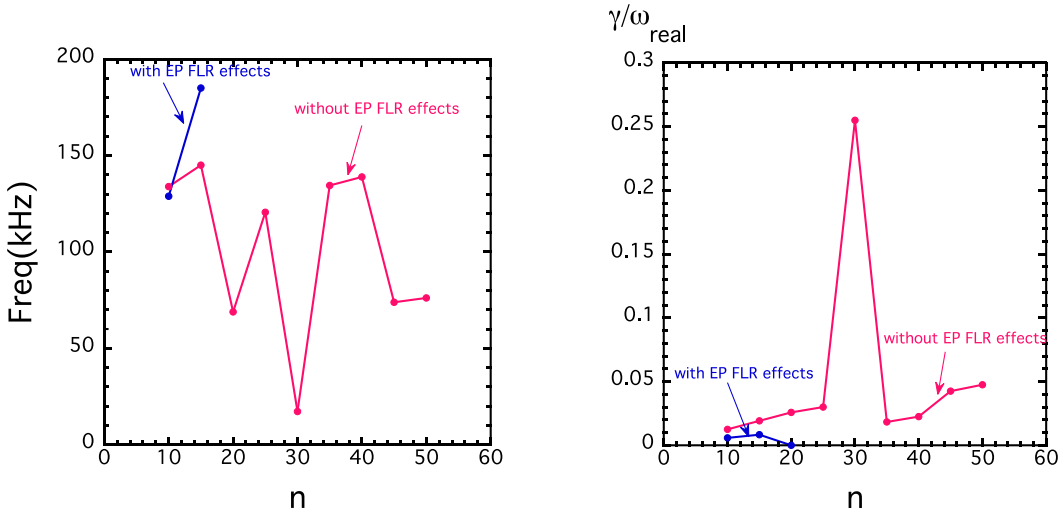

Fig. 6: *Frequency and growth rate in the ITER baseline 101006 case predicted by FAR3D with (blue) and without (red) finite-orbit effects.*

The observed unstable modes exist in the first geometrical continuum gap, consistent with identification as a TAE or RSAE (Fig. 7). For modes located near the q_{min} surface, the eigenfunction appears more TAE-like or RSAE-like depending on where a it lies along the RSAE frequency sweep

cycle defined by ($\frac{\left[m-\frac{1}{2}\right]}{n} < q_{\min} < \frac{\left[m+\frac{1}{2}\right]}{n}$). This can be seen in the electrostatic potential ϕ eigenfunctions in Figs. 8a and 8b, for n=10 and n=20 respectively. The n=10 eigenfunction (Fig. 8a) shows superposition of adjacent poloidal harmonics characteristic of TAEs. The n=20 eigenfunction is more RSAE-like, more dominated by a single poloidal harmonic.

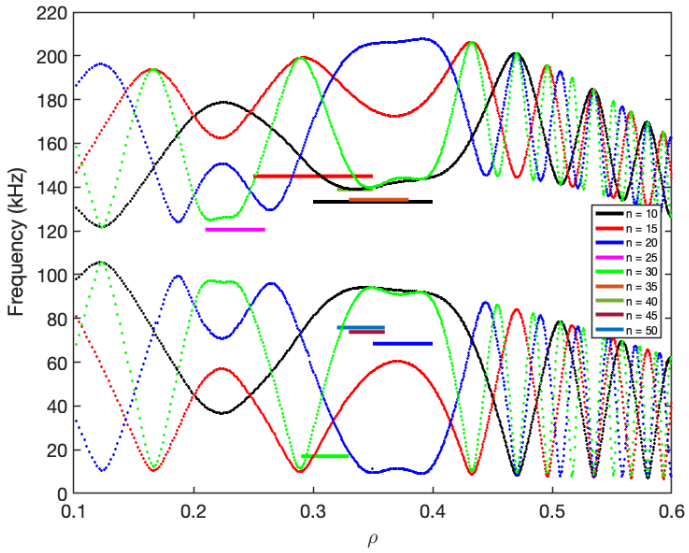

Fig. 7: *Alfvén continuum and predicted unstable modes as seen in the ITER baseline case by FAR3D. Other milestone participants have calculated near identical continuum spectra.*

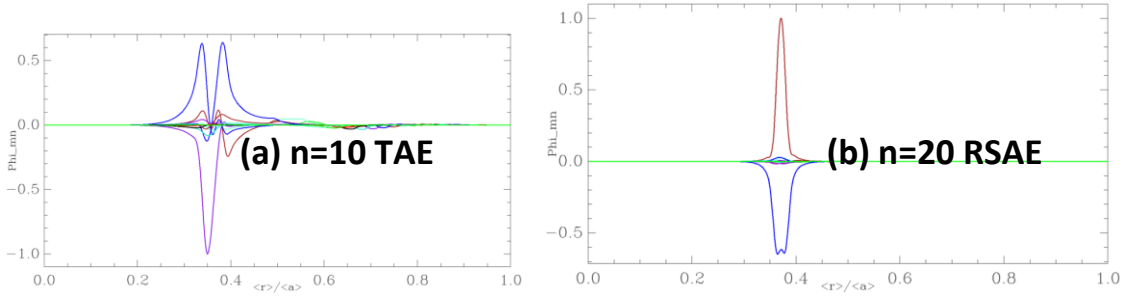

Fig. 8: *Poloidal harmonic decompositions of the electrostatic potential ϕ for (a) n=10 and (b) n=20 predicted by FAR3D for the ITER baseline case.*

Poloidal cross sections of potential f are generally non-ballooning (RSAE-like) or weakly ballooning (TAE-like) for modes at the $q_{\min}$ surface. One mode at n=25 peaks at the shallow $q_{\max}$ surface near axis is more strongly TAE-like, with a distinctly RSAE-like secondary peak at the qmin surface. See Fig. 9.

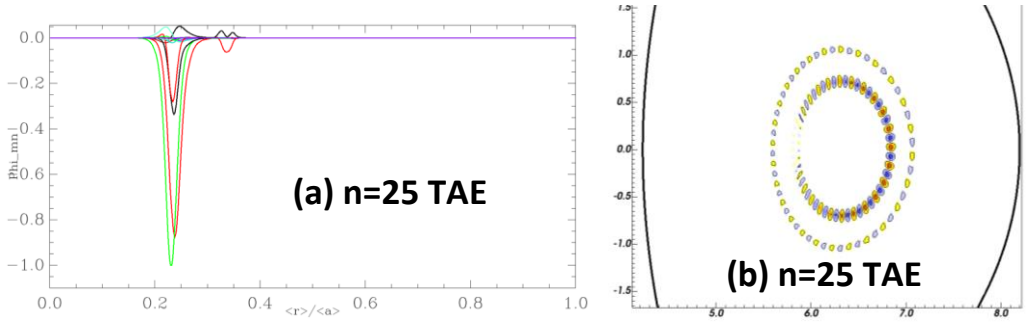

Fig. 9: *Poloidal harmonic decomposition (a) and cross section (b) of the n=25 TAE predicted by FAR3D in the ITER baseline scenario.*

M3D-C1 finds unstable AEs at 8≤n≤18, consistent with the FLR-inclusive FAR3D results but at much higher relative growth rates. This is especially the case since no enhancement of the EP drive was required in the M3D-C1 simulations. Figure 10 shows the M3D-C1 frequency and growth rate spectrum and the ϕ eigenfunction at n=9, the most unstable mode. The M3D-C1 simulations have used the realistic velocity-space distribution for this case and all others reported here.

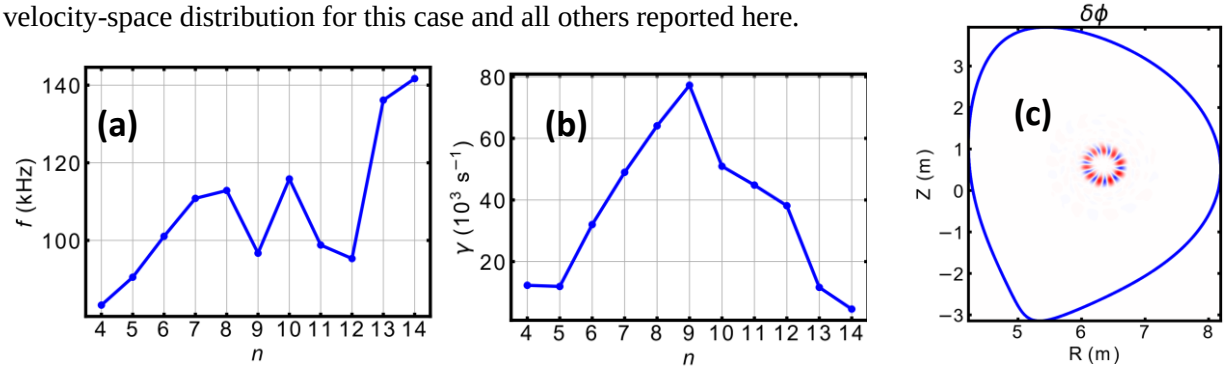

Fig. 10: *The AE linear frequency (a) and growth rate (b) from the ITER baseline case from M3D-C1. The BAE-like ϕ eigenfunction from the leading n=9 mode is shown in (c).*

GTC simulations find a BAE/RSAE-like mode with frequency and growth rate in Fig. 11(a) and the mode structure for n=19 in Fig. 11(b). GTC uses a local Maxwellian distribution for the beam ions in this simulation. Unstable AEs extend up to at least n=30 shown in Fig. 11 (c), where a more TAE-like mode with ballooning is seen.

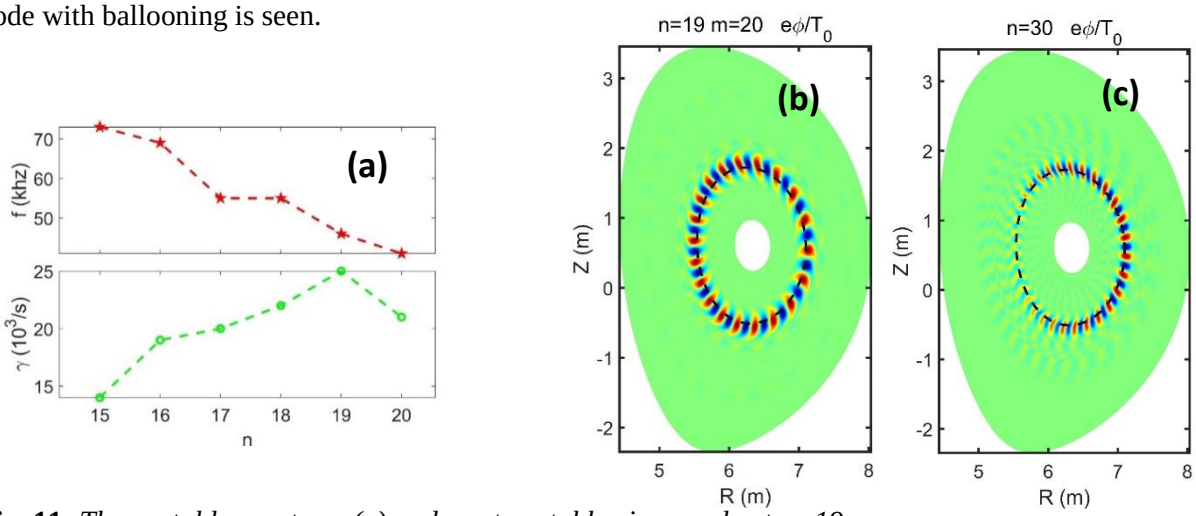

Fig. 11: *The unstable spectrum (a) and most unstable eigenmode at n=19, a BAE/RSAE-like mode, simulated in GTC for the ITER baseline case.*

Unstable RSAEs were seen in ORB5 in the absence of the NBI, presumably driven by thermal electrons. The strongest instability is seen at n=50. The identification of the modes as RSAE is based on spectrographic peaks relative to the Alfvén continuum as calculated by LIGKA (Fig. 12a) and poloidal decomposition of the main unstable n numbers (seen for n=50 in Fig. 12b). No other code with thermal-species kinetic physics has yet looked for similar thermal electron-driven RSAEs.

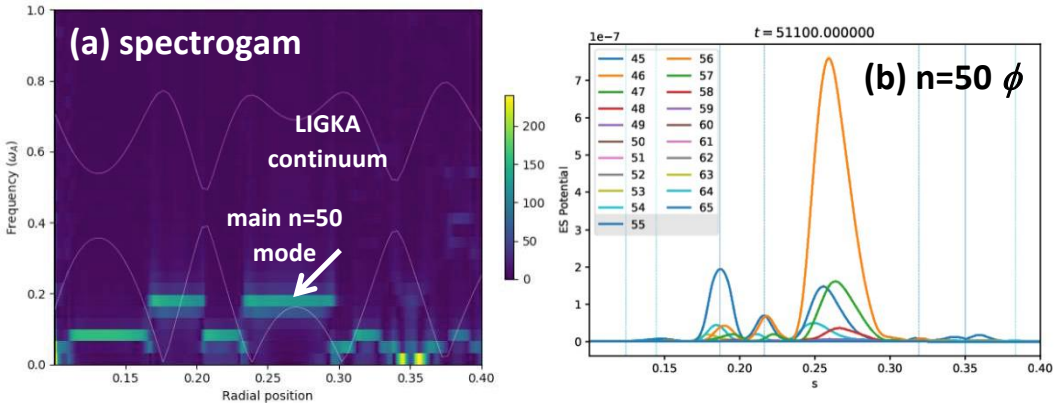

Fig. 12: *Thermal-electron driven RSAE seen by ORB5 at n=50 in the ITER baseline case as identified by (a) frequency spectrogram and (b) poloidal ϕ decomposition.*

4.1.2. DIII-D

The DIII-D shot 178631 baseline scenario has been simulated in GTC, GYRO, M3D-C1, and NOVA-K. The MHD hybrid code M3D-C1 sees apparent BAEs, while NOVA-K sees only TAEs. The kinetic codes both find leading modes in the TAE frequency gap, but sometimes disagree on the propagation direction and unstable n range. A rotation-inclusive continuum structure (and AEs) has been calculated in NOVA, shown in Fig. 13 at various n values for reference.

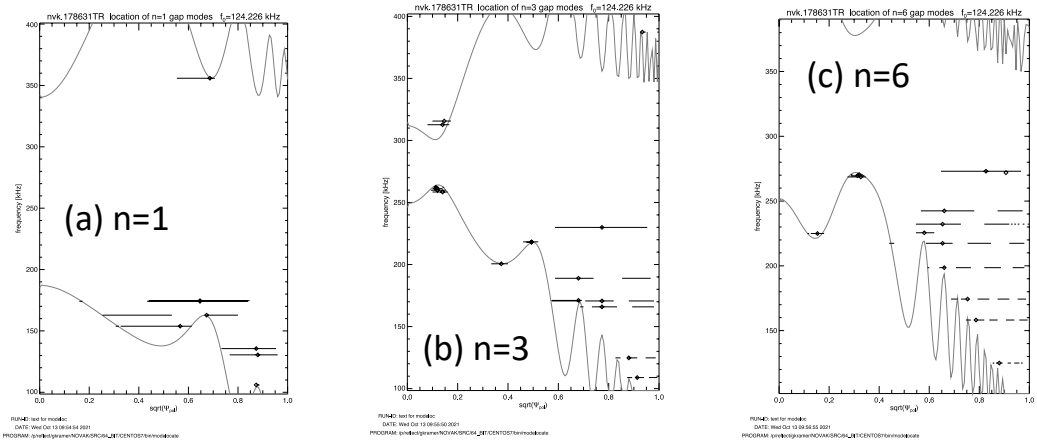

Fig. 13: *Alfvén continuum structure for (a) n=1, (b) n=3, and (c) n=6 and AEs calculated in NOVA with rotation included. These continuua are representative of results from other milestone participants.*

GTC simulation results are shown in Fig. 14. The peak growth rate is found at n=4, and all frequencies lie in the TAE continuum gap. A representative eigenmode at n=4 shows a radially-extended, phase-sheared, strongly ballooning structure.

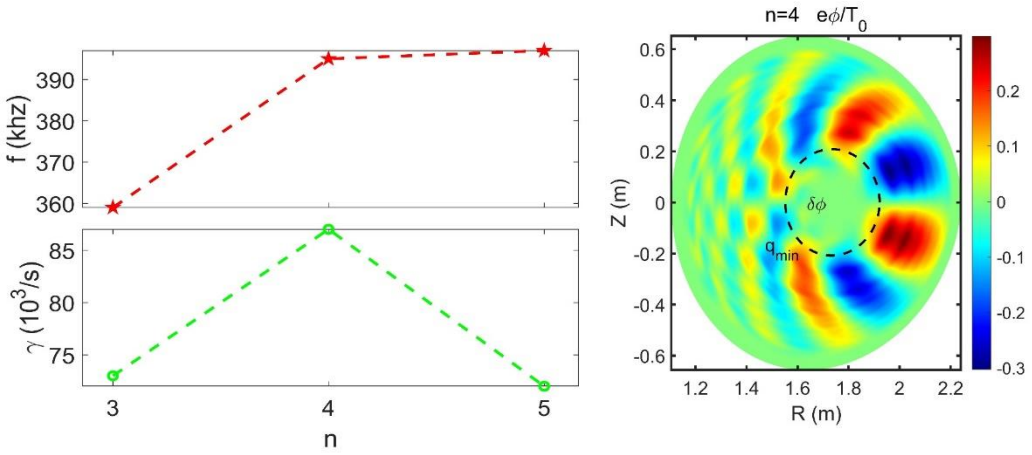

Fig. 14: *GTC unstable spectrum (a) and n=4 ϕ eigenfunction (b) for the DIII-D shot #178631.*

The same equilibrium simulated in GYRO shows unstable modes out to n=10 and likely somewhat beyond. Notably, at the low-n range unstable modes in GYRO are counter-propagating (electron diamagnetic direction), which has never before been reported for beam-driven AEs in GYRO. These results may indicate either that thermal electrons are involved in the drive or that the drift part of the resonance is of less importance than in cases studied previously. For n>5, modes present like typical BAE-RSAE-TAEs. Figure 15 shows the unstable spectrum and Fig. 16 shows two representative eigenfunctions. Large error bars in Fig. 15 indicate poor convergence in the initial-value simulation usually born of competing modes with close growth rates. To facilitate numerical stability, GYRO was run with collisional effects for this and the DIII-D steady-state case.

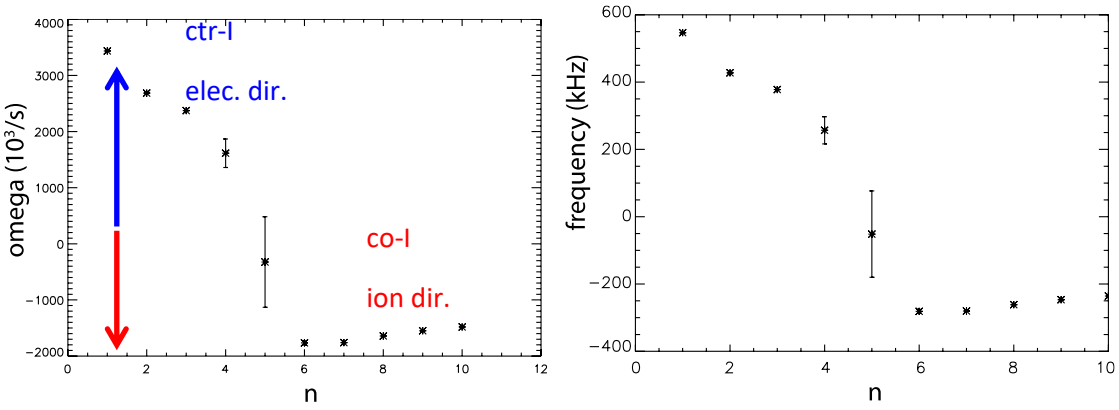

Fig. 15: *Unstable spectrum of modes simulated in GYRO for DIII-D shot 178631.*

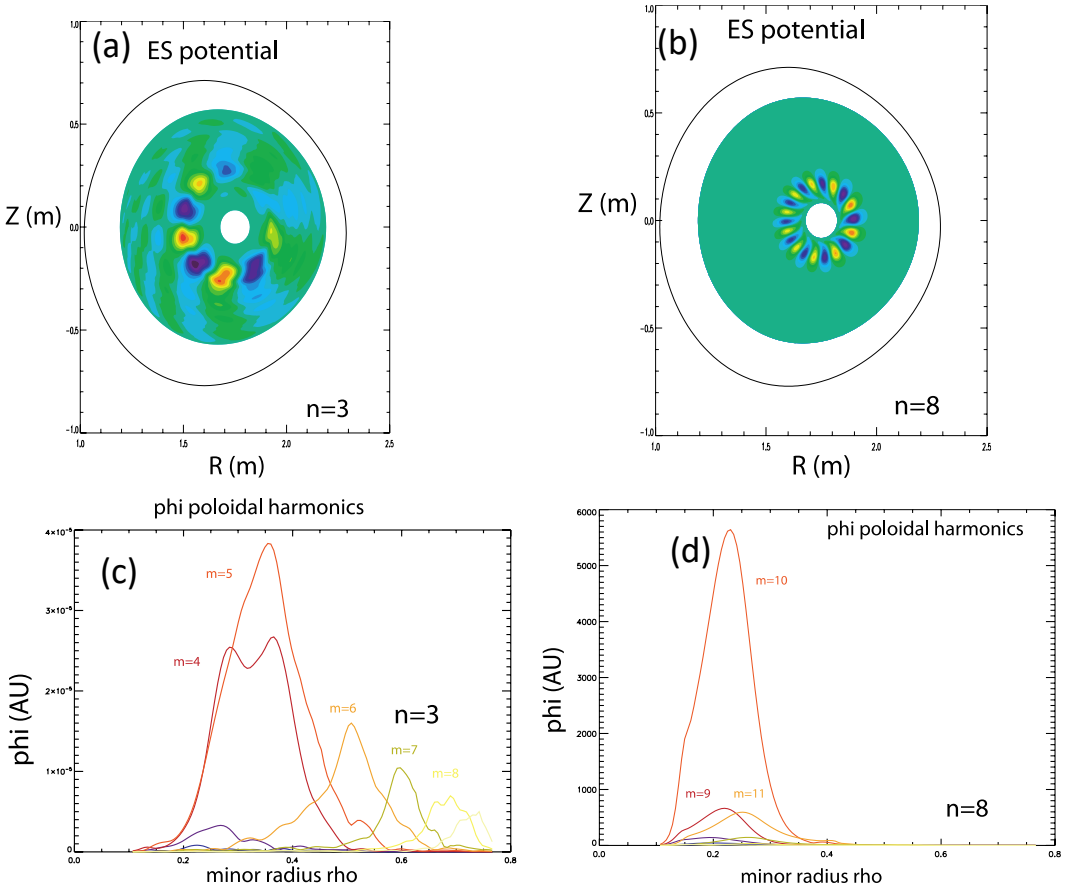

Fig. 16: *Representative eigenfunctions for co-propagating (a,c) n=3 and counter-propagating (b,d) n=8 modes simulated in GYRO for DIII-D shot 178631. The ϕ contours are shown in (a) and (b) and the poloidal harmonics in (c) and (d).*

Linear simulations in M3D-C1 predict RSAE-like modes at $8 \leq n \leq 11$, in rough agreement with GYRO in this range. Figure 17 shows the unstable spectrum and poloidal ϕ contours of the leading mode. Since the MHD calculation in M3D-C1 is performed self-consistently with the kinetic EP drive, the eigenfunctions exhibit mode phase shearing characteristic of these modes, seen in the ϕ eigenfunction in Fig. 17c.

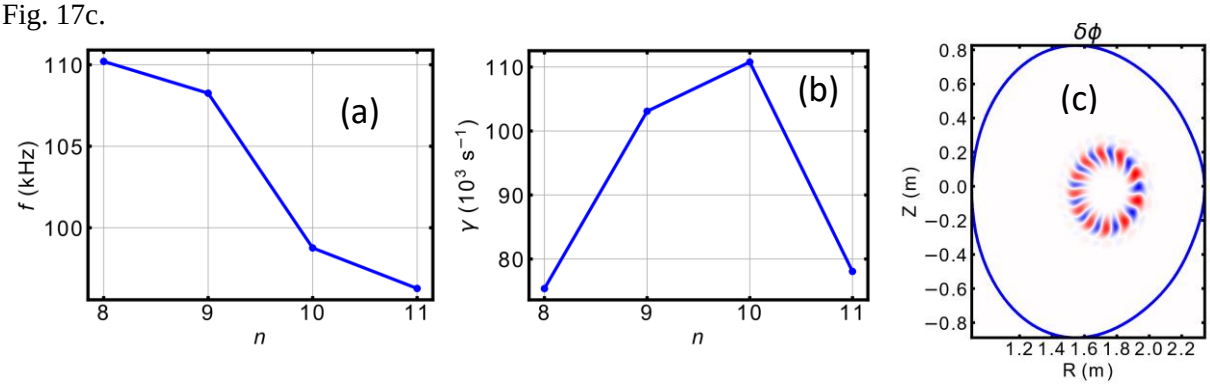

Fig. 17: *Frequency (a), growth rate (b), and ϕ eigenfunction (c) of unstable n=10 RSAE seen in M3D-C1 simulations of DIII-D shot # 178631.*

NOVA-K has been applied with varying models. Without rotation, both an isotropic slowing-down distribution and one peaked in pitch angle have been used. Only TAEs were observed across n values. The rotation-inclusive Summaries in Fig. 18 and Fig. 19.

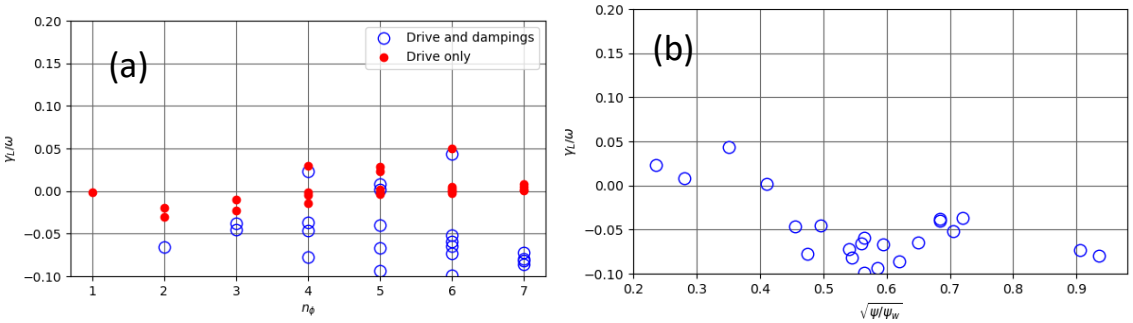

Fig. 18: *NOVA-K calculations of TAE growth rate vs. (a) frequency and (b) mode peak location with an isotropic slowing-down EP distribution in DIII-D shot #178631.*

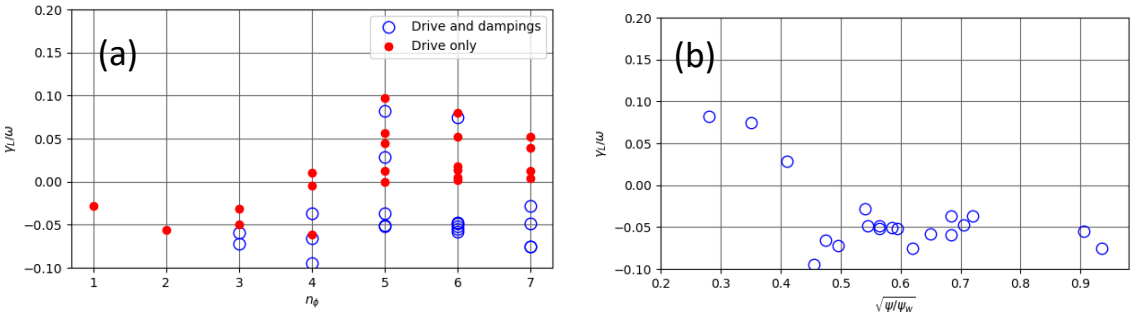

Fig. 19: *NOVA-K calculations of TAE growth rate vs. (a) frequency and (b) mode peak location using a slowing-down EP distribution with a peak at the injection pitch angle in DIII-D shot #178631.*

4.2. Steady state scenario

The ITER steady-state case 131041 has been examined by GTC, FAR3D, M3D-C1 and MEGA. Unstable modes in FAR3D, at 8≤n≤12, are all anti-ballooning ellipticity-induced Alfvén eigenmodes (EAEs). The other codes see typical TAEs or RSAEs. The DIII-D steady-state case 132710 has been examined by GYRO, and M3D-C1. AE growth rates peak around n=7,8 in GYRO simulation. However, M3D-C1 simulations see no instability.

4.2.1. ITER

FAR3D simulations of the ITER steady-state case 131041 have, so far, only shown modes in the ellipticity-induced Alfvén eigenmode (EAE) gap. Fig. 20 shows the n=20 Alfvén continuum as calculated in FAR3D. It is representative of continua calculated by other milestone participants. Fig. 21 shows the unstable spectrum calculated in FAR3D for this case, with frequencies in the EAE gap and poloidal contours of a representative eigenmode at n=10 showing anti-ballooning behavior exhibited by all observed modes.

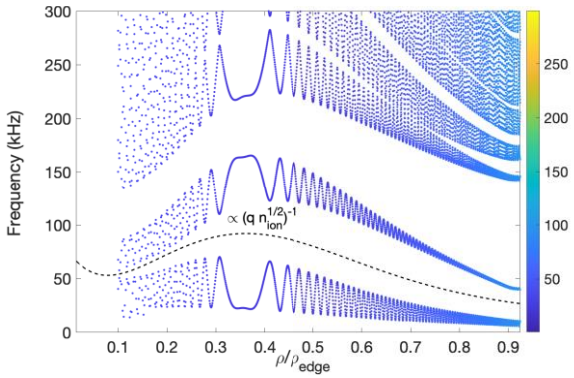

Fig. 20: *Alfvén continuum spectrum for the ITER steady-state case calculated in FAR3D.*

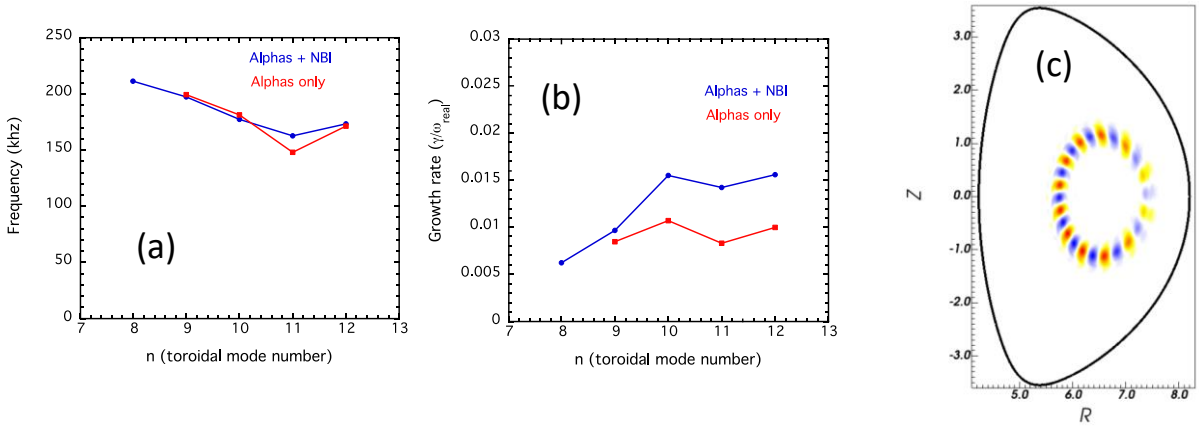

Fig. 21: *Frequency (a) and growth rate (b) of unstable AEs in FAR3D for the ITER steady-state case. Poloidal ϕ contours of the n=10 instability show anti-ballooning exhibited by all observed modes.*

Unstable modes in GTC, by contrast, are universally TAE-like for this case. A fully realistic EP distribution was used for this case: anisotropic slowing down for neutral-beam ions and isotropic slowing down for alpha particles. The continuum spectrum for n=10 mode is shown in Fig. 22. Figure 23 shows the unstable spectrum and the n=30 eigenmode showing TAE-like ballooning behavior.

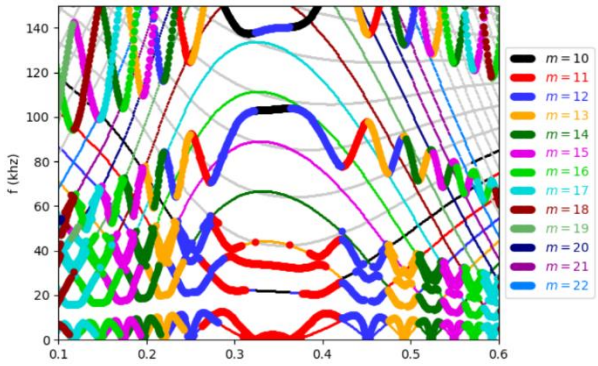

Fig. 22: *Alfvén continuum spectrum for the ITER steady-state case calculated in GTC.*

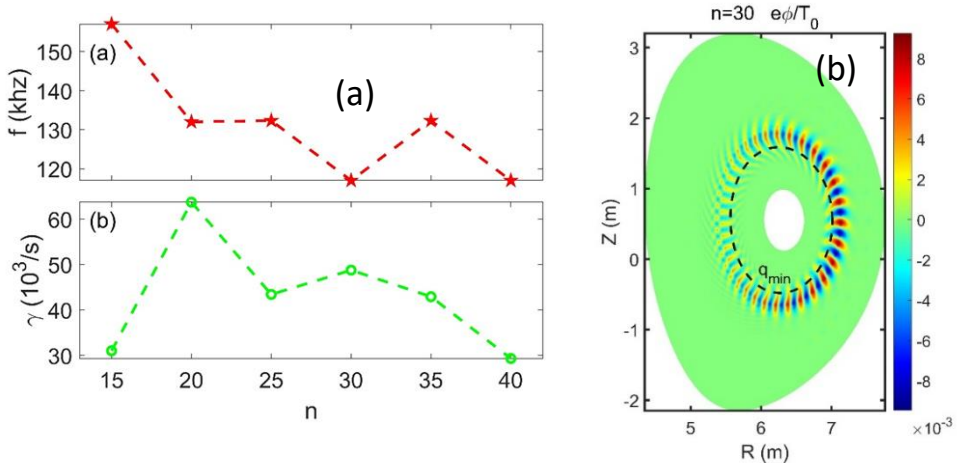

Fig. 23: *Unstable spectrum (a) and poloidal ϕ contours of the n=30 eigenmode (b) calculated in the GTC code for the ITER steady-state case.*

An unstable TAE is also identified in MEGA at n=15. Figure 18 shows poloidal ϕ contours (Fig. 24a) and harmonics (Fig. 24b).

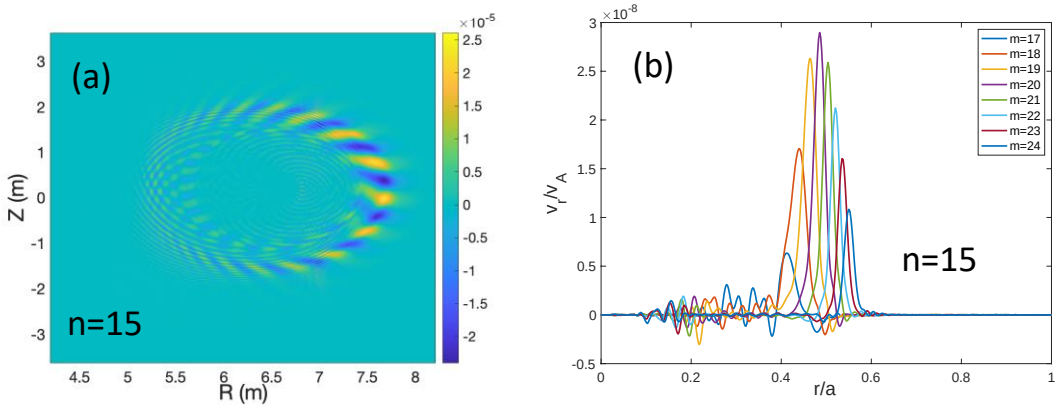

Fig. 24: *Poloidal ϕ contours (a) and m of harmonics of a TAE calculated in MEGA at n=15 for the ITER steady-state case.*

M3D-C1 has identified three distinct unstable AE branches for the ITER stead-state case: an RSAE at the lowest unstable n values and two distinct TAEs at the higher unstable n vales. Figure 25a shows frequency plotted versus n, with discrete jumps in frequency. Growth rates in Fig. 25b show that the lower-n RSAEs dominate the spectrum, with less distinct TAE peaks at higher n. Exemplars of eigenfunctions of each branch are seen in Fig. 26.

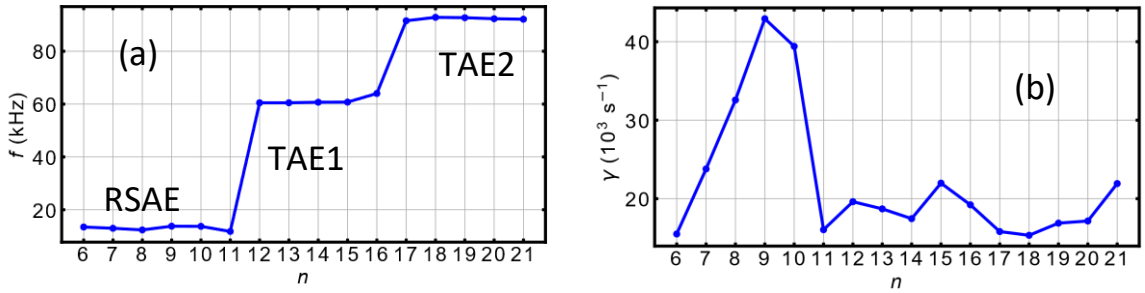

Fig. 25: *Frequency (a) and growth rate (b) of unstable AEs in simulated in M3D-C1 for the ITER steady-state case showing three distinct branches.*

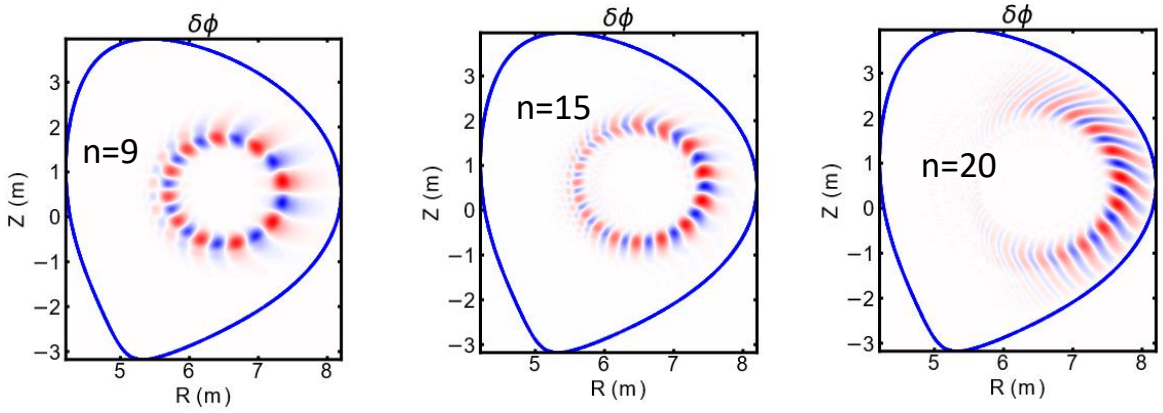

Fig. 26: *Electrostatic potential eigenfunctions of (a) an RSAE at n=9, (b) a TAE at n=15, and (c) a second TAE at n=20 simulated in MSD-C1 for the ITER steady-state case.*

4.2.2. DIII-D

Linear GYRO simulations identify BAE/RSAE-like modes in the range $6 \leq n \leq 9$, with poor convergence at other n values simulated. The unstable spectrum (Fig. 27a) is consistent with RSAEs somewhere in the sweep range between the BAE and TAE frequencies. The eigenfunction at the leading n=8 (Fig. 27b) shows single-harmonic dominance, consistent with BAEs or RSAEs near the lower end of the frequency sweep.

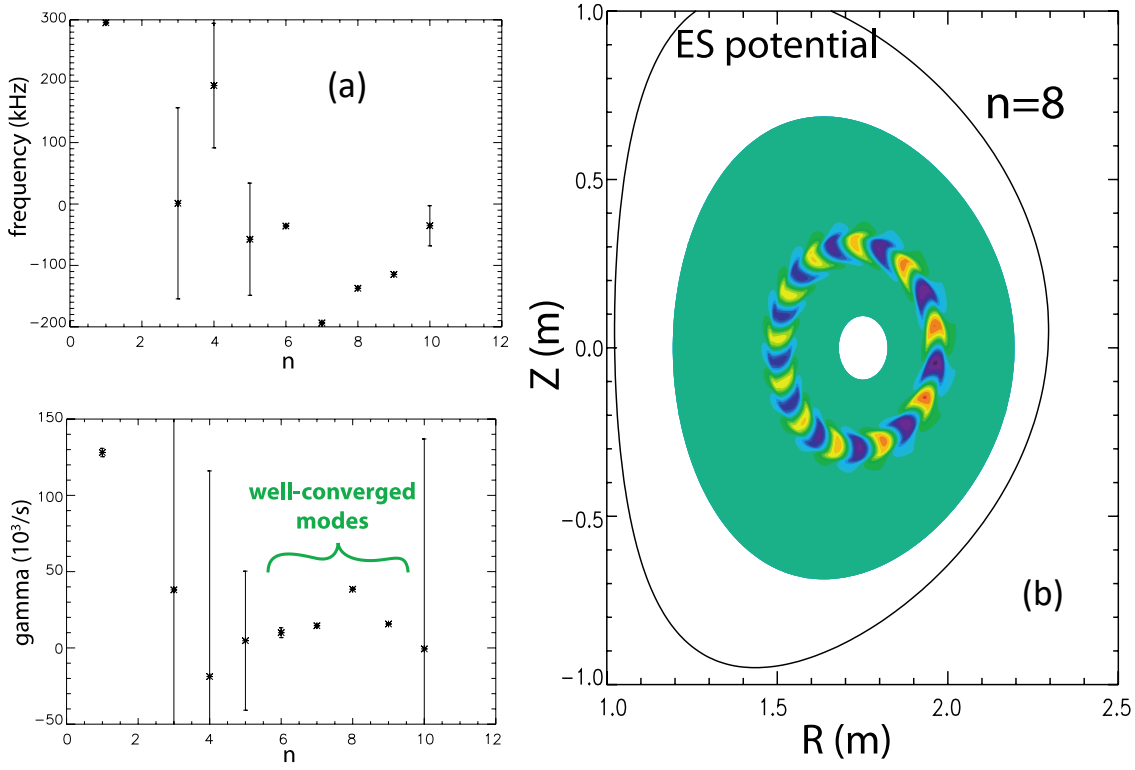

Fig. 27: *Unstable spectrum (a) and ϕ eigenfunction of the leading n=8 eigenmode (b) showing BAE/RSAE-like single-harmonic dominance (minimal ballooning) simulated in GYRO for the DIII-D steady-state case.*

5. Microinstability (drafted by X. Wei)

In **GTC** (X. Wei) electrostatic simulations, the equilibrium distribution functions of the thermal ion and the electron are local Maxwellians, and the equilibrium distribution function of the energetic particles is isotropic slowing down distribution with the injection energy as the birth energy of particles. GTC finds electrostatic trapped electron mode (TEM) or ion temperature gradient (ITG) mode in the four cases. Table 1 briefly lists the main results of the linear drift wave instability in the four cases.

Table 1 Main results from the electrostatic simulations

	ITER baseline #101006	DIII-D #178631	ITER steady-state #131041	DIII-D #132710
Simulation grids ($N_\psi \times N_\theta^{\max} \times N_\parallel$)	$500 \times 6268 \times 32$	$300 \times 682 \times 32$	$550 \times 5842 \times 32$	$300 \times 680 \times 32$
Main instability	TEM	TEM	ITG mode	TEM
Growth rate (s^{-1})	2.89×10^4	1.38×10^5	1.01×10^5	9.39×10^4
Mode frequency (s^{-1})	6.12×10^4	1.61×10^5	-7.91×10^4	7.84×10^4
$k_\theta \rho_i$ for the maximum amplitude	0.74	1	0.70	0.55
Poloidal harmonic m	150-450	40-60	150-350	35-75
Toroidal mode n	100-250	30-50	75-150	20-50

5.1. Baseline scenario

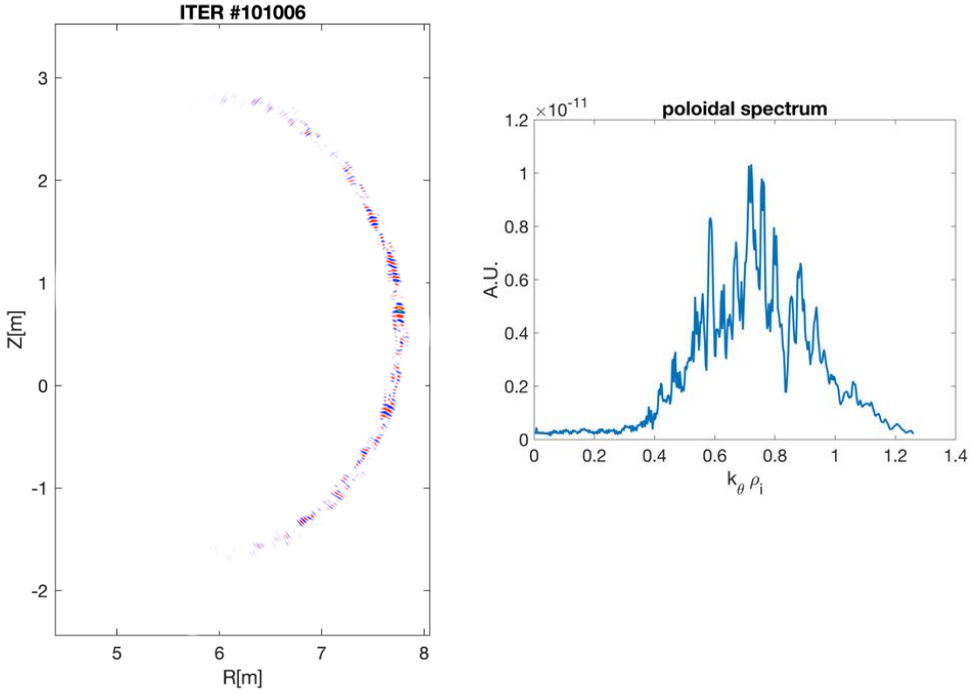

Fig. 28 *Linear poloidal mode structure (left) and spectrum (right) from GTC simulation of ITER #101006.*

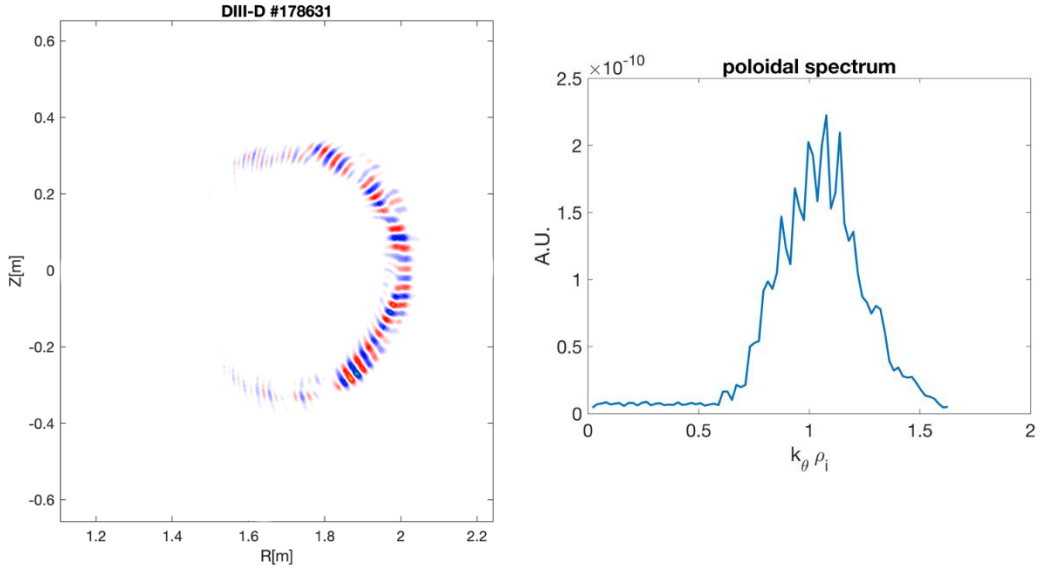

Fig. 29 *Linear poloidal mode structure (left) and spectrum (right) from GTC simulation of DIII-D #178631.*

5.2. Steady state scenario

Only the thermal ions (Deuterium) and the beam ions(Protium) are included in the simulation and the alpha particles are not included. $P_{NBI}/P_{\alpha} \approx 1/1.8$ at the magnetic axis.

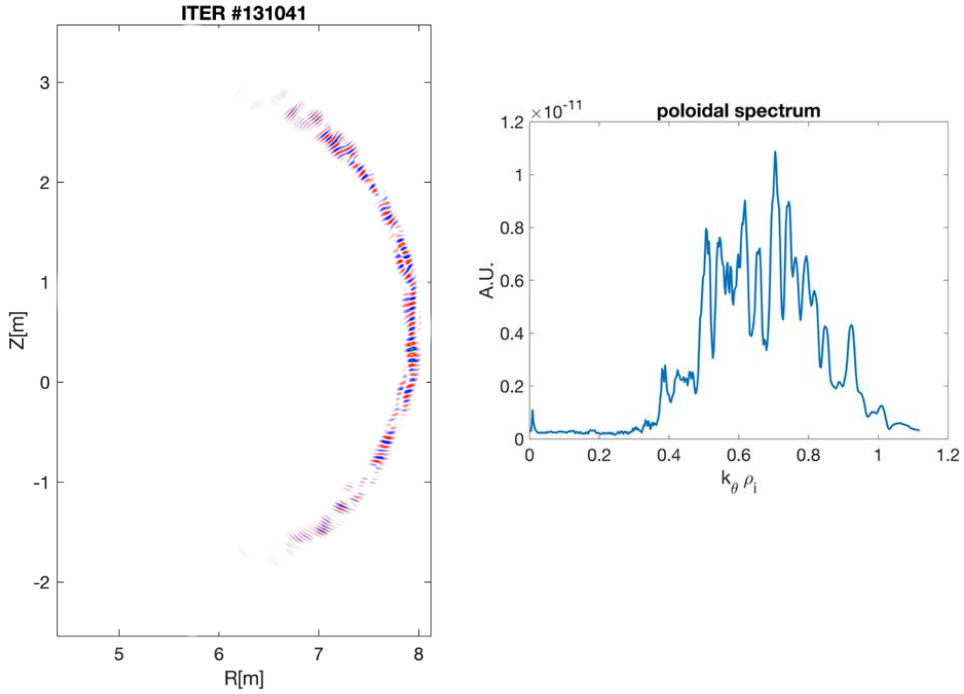

Fig. 30 *Linear poloidal mode structure (left) and spectrum (right) from GTC simulation of ITER #131041.*

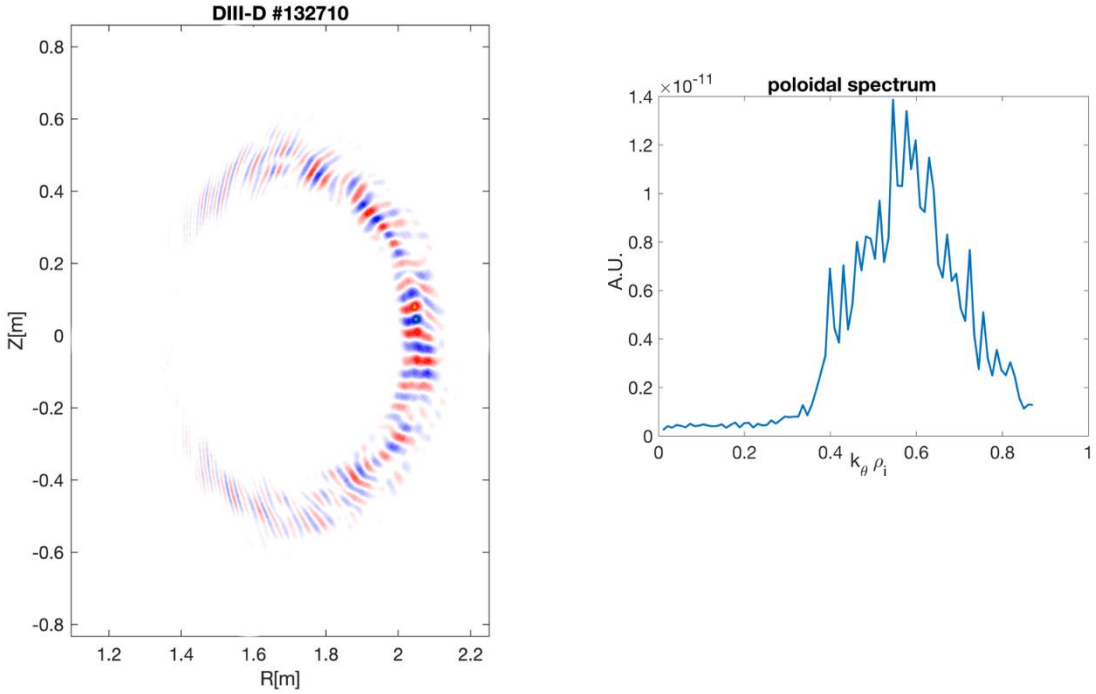

Fig. 31 *Linear poloidal mode structure (left) and spectrum (right) from GTC simulation of DIII-D #132710.*